







Millimeter-Wave Radar Sensor for Automated Tomographic Imaging of Composite Materials in a Manufacturing Environment

Dominik Meier¹ , Christian Zech¹ , Benjamin Baumann¹, Bersant Gashi¹ ,
Matthias Malzacher¹, Michael Schlechtweg¹, Jutta Kühn¹ , Markus Rösch¹ ,
and Leonhard M. Reindl² 

¹Fraunhofer Institute for Applied Solid State Physics IAF, 79108 Freiburg, Germany

²University of Freiburg Department of Microsystems Engineering IMTEK, 79110 Freiburg, Germany

Manuscript received November 20, 2020; revised January 20, 2021; accepted January 22, 2021. Date of publication January 28, 2021; date of current version February 23, 2021.

Abstract—To unlock the full potential of composite materials, reliable measurement methods during and after their manufacturing are required. Established measuring methods are commonly based on ultrasound or thermographic imaging techniques and offer only a limited usability. A promising alternative to the aforementioned methods are millimeter-wave-based systems. It has already been demonstrated that such systems can provide a tomographic representation of composite materials, enabling the detection, localization, and classification of critical defects within the component. The tomographic millimeter-wave imaging system presented here is operating in the W band and is packaged for the operation in a manufacturing environment. For this purpose, it is enclosed by a dustproof housing and can be mounted on an industrial robot, which enables the development of an automated measurement procedure during and after the manufacturing process of composite materials. The direct integration of the measurement system into the manufacturing process allows for early-stage fault detection and classification, which is essential for the production of high-quality, high-performance, and highly reliable composite materials.

Index Terms—Microwave/millimeter wave sensors, composite materials, millimeter-wave (mmW) radar, nondestructive testing, radar imaging, robot programming.

I. INTRODUCTION

The properties of composite materials can be adjusted to the requirements of the respective tasks, by altering their mechanical or chemical properties through the selection of different constituents and their mechanical layout. Especially the strength-to-weight ratio of certain composite materials, such as glass-fiber reinforced plastics (GFRPs), makes them an excellent choice in a wide field of applications. These include ships, aircrafts, trains, cars, storage tanks, wind turbines, and many more [1]. To make use of the full potential of such materials, they have to be defect free. Especially in the case of large-sized structures, which are mainly manufactured by manual craftsmanship, a defect-free component cannot be guaranteed without the application of a proper inspection method. High-performance components require reliable methods to assure their quality and enable the detection and classification of any critical defect during and after the manufacturing process. Ultimately, such a measurement method enables the manufacturing of stronger, yet lighter components, which is a key factor in achieving more efficient, more reliable, and more sustainable systems. Ensuring a defect-free material allows for the thickness and strength requirements of said material to be lowered, the thickness of the components can be reduced while they still provide the required mechanical strength.

The currently established measurement methods for the inspection and investigation of GFRP have their individual limitations with regard to tomographic material inspection [2], [3]. While ultrasonic-based methods are capable of generating a tomographic representation of GFRP, the requirement of a coupling medium, that may possibly react

with uncured resin and destroy the measured components, limits their usefulness in a manufacturing environment. The tomographic information acquired via thermographic methods is restricted to only limited depth information, due to the measurement principle. X-rays-based methods are rarely used in a manufacturing environment, due to their ionizing radiation. Finally, methods utilizing the optical or terahertz frequency spectrum typically have a limited penetration depth, due to the materials' absorption coefficient increasing with frequency.

It has already been shown that systems based on millimeter waves (mmW) can be used for nondestructive material inspections [4]–[6], since they provide a sufficient resolution to detect, localize, and classify critical defects in GFRP, which are used as force compensating components. This contact-less and nondestructive method can be deployed at any point in the manufacturing chain. This enables the direct detection through live monitoring. In this letter, an mmW-based measurement system, with focus on applicability in a manufacturing environment, is presented.

The structuring of this letter is as follows: Section II provides the basic working principle of mmW-based tomographic imaging. Section III presents the mmW imaging system for the automated investigation of composite materials. This is followed by measurement results of a composite material with incorporated defects, which are presented in Section IV, and finally, Section V concludes this letter.

II. MILLIMETER-WAVE TOMOGRAPHIC IMAGING

The basic procedure to generate mmW-tomographic images of composite materials is comparable to those applied in ground-penetrating radar or wall-penetrating radar techniques [7], [8]—with the system

Corresponding author: Dominik Meier (e-mail: dominik.meier@iaf.fraunhofer.de).
Associate Editor: X. Shu.
Digital Object Identifier 10.1109/LENS.2021.3055060

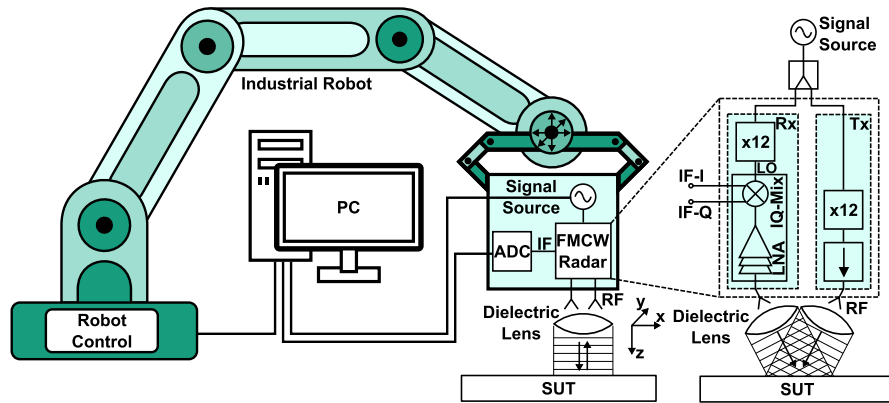


Fig. 1. Schematic depiction of the measurement system, including radar front end, a robotic arm providing the motoric movement, data processing, and movement control. The inset on the right-hand side of the image shows the radar front end in more detail.

presented here being based on the frequency-modulated continuous-wave (FMCW) radar principle. Yet, in contrast to a classical radar application, in which the distance of a target is detected, the distance to the sample under test (SUT) and its thickness are already known. The tomographic information of interest of the composite material is encoded in the received signal's magnitude and phase within the frequency range corresponding to the SUT's range position [5].

In a typical composite material, the reflected mmW signal is a combination of multilayer reflections from the individual fiber layers, excited radiating coupled modes, and reflections from any dielectric interface boundary—which could be the sample's top-surface, backside, or a deviation in the component's layout [9]. Based on this information, the detection of inhomogeneities in the material's internal structure, like fiber perturbations or variations in the relative fiber-to-resin volume ratio in GFRP, becomes possible. Considering that the fiber orientation in such systems is the defining factor of the material's mechanical strength, such measurement systems can provide vital information on the sample's quality, while also revealing weak points in its internal structure.

In such an FMCW system, the radar resolution

$$\Delta R_R = \frac{c_m}{2B} \quad (1)$$

is defined by the speed of light c_m in the investigated medium and the radar signal's bandwidth B . This resolution defines the minimal distance between two separate targets for them to be distinguishable. In the case of an intensity-based evaluation, as presented in this work, the range accuracy is approximately proportional to $(B^2 N \eta)^{-1}$ [10] and depends, besides the radar bandwidth, on the signal-to-noise ratio (SNR) η and the number of samples N recorded by the analog-to-digital converter (ADC). As shown in [5], a phase-based evaluation can also be a viable approach. The achievable lateral resolution depends on the wavelength of the utilized radar signal and the antenna front end. The achievable penetration depth of the signal depends on the material's absorption coefficient and on the radar's dynamic range. Typically, this results in the following premise: While a higher frequency, typically resulting in a higher bandwidth, of the radar signal provides an enhanced resolution, at the same time, the signal attenuation increases as well, limiting the signal's penetration depth into the material. Keeping this in mind, the optimal frequency range of the radar depends on the SUT's dielectric properties, its size, and the resolution required to resolve defects that are classified as critical for the target application [11].

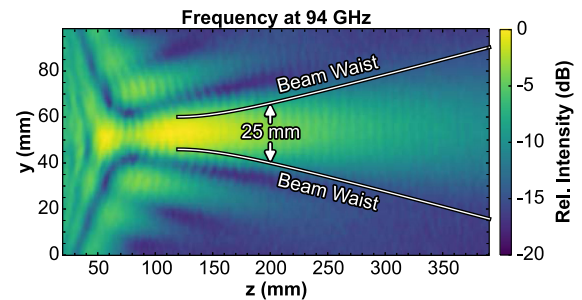


Fig. 2. Measured near-field pattern of the 15-dBi rectangular horn antenna in combination with the designed HDPE lens used for the radar front end.

III. MEASUREMENT SYSTEM

A schematic depiction of the developed measurement system can be seen in Fig. 1. In order to generate the radar signal, a custom-made phase-locked loop is utilized as a signal source. With it, linear frequency chirps from 6.85 to 8.85 GHz, with a pulse duration of 1.04 ms, are generated. A power splitter divides the generated signal into the transmit-and-receive signal. Both, the transmitter and the receiver, consist of a frequency multiplier-by-twelve (x12) [12] each, which up-converts the source signal into W band—providing a suppression of unwanted harmonics of more than 25 dBc within the 3-dB bandwidth frequency range of the x12. With the used frequency chirps, this results in an operational bandwidth of 24 GHz. While no further active components are used in the transmit path, the receiver consists of an IQ-mixer with an integrated low-noise amplifier (LNA). The components used in the transmit and receive path are based on the Fraunhofer IAF's 100-nm metamorphic HEMT (mHEMT) process [13] and are assembled in WR10 waveguide split block modules.

The mmW signal is focused onto the SUT by using a 15-dBi rectangular horn antenna in combination with a high-density polyethylene (HDPE) lens. This front-end setup is identical for both the transmit and receive path. With this setup, a spot size diameter of 25 mm is achieved at a range of 200 mm from the lens tip. This is confirmed by the measurement of the antenna lens combinations near-field pattern within the W band, which is shown in Fig. 2 for a frequency of 94 GHz. The near-field measurement shows the radiation pattern of the transmitter, with the area of interest being scanned with a W band near-field probe connected to a spectrum analyzer. Due to the identical

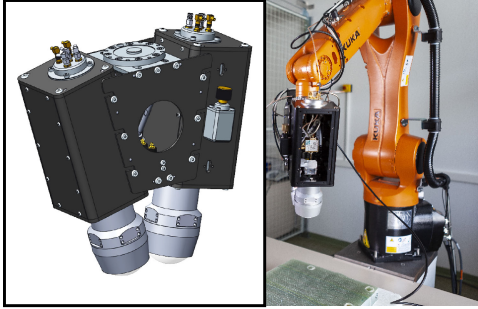


Fig. 3. Depiction of the radar-sensor housing can be seen on the left-hand side. An image of the mounting tool connected to the industrial six-axis robot is shown on the right-hand side.

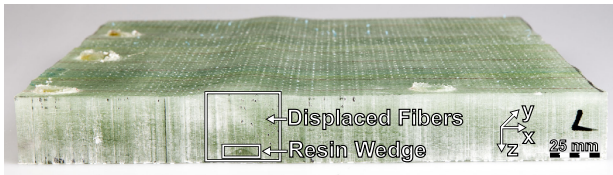


Fig. 4. Photo of the SUT with incorporated resin wedge.

antenna lens layout of the transmitter and the receiver, the radiation pattern of the receiver is similar in shape. Transmitter and receiver are integrated into a dustproof robotic-arm radar-mounting tool, which is designed to be attached onto an industrial robot. A 3-D rendered representation of this mounting tool is shown in Fig. 3 on the left-hand side. The housing is designed in such a form that the transmit and receive signal paths overlap at a distance of 200 mm.

An ADC with a sample rate of 15.625 MS/s and a resolution of 14 bit is used to record the detected intermediate frequency (IF) signal, which is then stored for offline processing. The radar front end, together with the signal source and the ADC, is integrated, respectively, connected to the mounting tool. A KUKA KR 10 R1100 sixx six-axis industrial robot is used to scan the SUT, which enables the position and alignment of the radar front end to be freely adjustable in a 3-D space, to match the requirement of the specific SUT. The radar tool, attached to the utilized robotic arm, can be seen in Fig. 3 on the right-hand side. In the photo, the side plate of the radar housing, on which the ADC is connected, is removed in order to reveal the internal split block modules.

IV. MEASUREMENT RESULTS

To demonstrate the radar-based imaging system, a GFRP sample with integrated defect, in the form of a resin wedge, with a width of 18 mm and a height of 4 mm, is measured. A photo of the 300 mm × 300 mm × 40 mm large SUT can be seen in Fig. 4. The position of the resin wedge is marked, it being approximately 35 mm below the surface and stretching over the complete 300-mm length of the SUT. The displaced fibers, resulting from the distorted fiber layers located on top of the wedge insert, are also marked. The material composition and structural layout of the SUT corresponds to the structure of wind turbine spar caps, which provide the mechanical stability of wind turbine rotor blades. The SUT has a relative fiber-to-resin volume ratio of 0.8, composed of a monoaxial fiber layout with a fiber diameter of 17 μm.

The data processing to generate a tomographic representation of the SUT is performed in a similar way as described in [5], with the

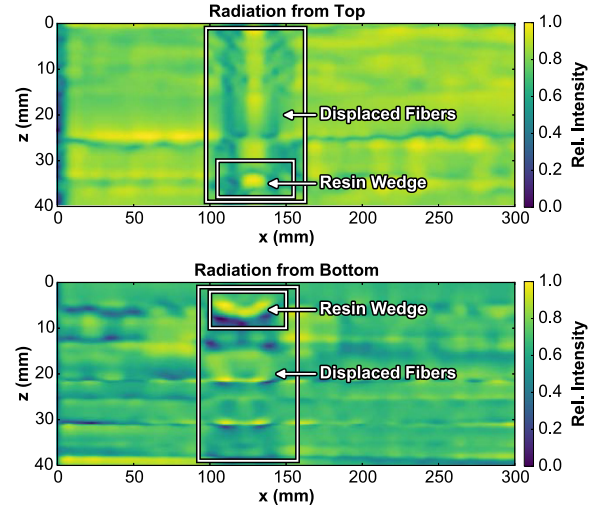


Fig. 5. Measured cross section of the SUT. In the top diagram, the radar sensor is illuminating the top side of the SUT, while in the bottom diagram, the bottom side is illuminated.

key differentiating factor, that in this application an intensity-based evaluation, is performed. By transforming the recorded data of a single measurement position into the frequency domain using the chirp- Z transformation, the frequency range of the transformation can be set accordingly to fit the SUT's range and thickness. In the next step, the signal is transformed into the range domain using

$$R = \frac{c_m f_{IF} T}{2B}, \quad (2)$$

with R denoting the range, f_{IF} the received IF frequency, and T the frequency chirp's ramp duration. The result is an A-scan of the respective measured position. In the results shown here, the separate range bin layers' magnitude is normalized to the respective maximum value, in order to compensate for the clutter introduced by the surface reflection and also to compensate for the sample's signal attenuation.

By combining adjacent A-scans along a line, a B-scan can be generated. Such scans of the xz -plane of the SUT, with a step size of 2 mm along the x direction, are shown in Fig. 5. With the robot running in a manual-mode safety setting, the measurement of one cross section takes 2 min, limited by the mechanical positioning speed. The top diagram shows a measurement with the SUT facing upwards, while at the bottom diagram the SUT is facing downwards. In both images, the resin wedge, as well as the displaced fibers, are marked and can both be identified visually in the radar images. In the case of the resin wedge, a localization of the defect is possible as well as the determination of the defects shape and size. This allows for the possible classification of the defect in terms of its impact on the mechanical properties of the SUT. By scanning the SUT from both sides, the system's capability of detecting and classifying defects directly below the surface, as well near the backside is demonstrated.

By scanning the surface area of the SUT, a C-scan is generated. The diagrams in Fig. 6 show the xy -plane in various depths, scanned with a step resolution of 2 mm. While the top diagrams represent the measurement result with the SUT's topside facing upwards, the bottom diagrams are with the SUT being placed upside down. The left-hand side diagrams show the xy -plane in a depth corresponding to 5 mm below the SUT's respective surface layer. This corresponds to the resin wedge's position in the case of SUT being placed upside down. In contrast, the right-hand side diagrams represent the xy -plane at a depth of 35 mm below the current surface layer of the SUT. This

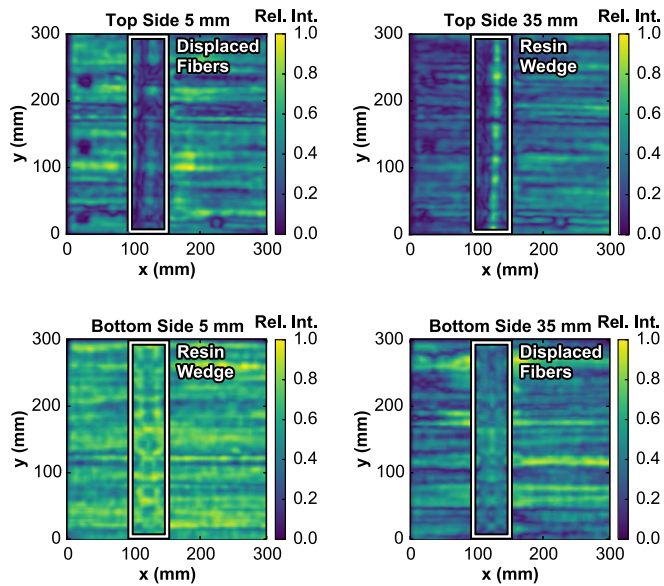


Fig. 6. Tomographic representation of the SUT, with the top side of the SUT illuminated by the radar on the top diagrams and the bottom side on the bottom diagrams. The left-hand side shows the xy -plane 5-mm below surface and the right-hand side 35-mm below surface.

time, this corresponds to the resin wedge's position in the case of the SUT being placed facing upwards. As can be seen in all scenarios, the resin wedge, as well as the distorted fibers, can be distinguished from the defect-free regions, enabling a detection of defects within the SUT and a classification of their extend.

V. CONCLUSION

In this letter, an mmW imaging system operating in the W band is demonstrated. The contact-less measurement system is capable of generating tomographic images of samples made of GFRP. The system enables detection, localization, and classification of critical defects for such components' mechanical stability. By integrating the radar front end into a dustproof housing with integrated dielectric lenses, the system can be operated in a manufacturing environment. As shown, by connecting the radar sensor with an industrial robot the measurement can be automated and could be integrated directly into the manufacturing process.

Further enhancements of the system, like increasing the amount of sensors to reduce the measurement time required or advanced data processing algorithms in order to enable automatic evaluation of the radar images, represent some of the next steps in order to further optimize the system for an industrial use. The sensor described in

this letter is operating in the W band, but it could be replaced with one capable of operating at higher frequencies in order to increase the image resolution if required, with the drawback of a reduced penetration depth for a given transmit power and receiver sensitivity. Additionally, a combination of different measurement principles, like thermography and mmW, can bring further benefits in the form of thermographic large-area error detection and mmW-based error classification. Overall, as demonstrated here, mmW-based measurement methods can provide a valuable addition to the tool box of composite material inspections.

ACKNOWLEDGMENT

The authors would like to thank Enercon and Composite Material Supply GmbH in Aurich for providing the samples under test, especially Torsten Link. They would also like to thank M. Zink from the Fraunhofer IAF for designing the mechanical components of the mounting tool. This work was supported by the German Federal Ministry of Economic Affairs and Energy (BMWi) in the frame of the InFaRo project under Grant 0324055 A.

REFERENCES

- [1] A. D. B. L. Ferreira, P. R. O. Nóvoa, and A. T. Marques, "Multifunctional material systems: A state-of-the-art review," *Composite Struct.*, vol. 151, pp. 3–35, 2016.
- [2] C. Garnier, M.-L. Pastor, F. Eyma, and B. Lorrain, "The detection of aeronautical defects in situ on composite structures using non destructive testing," *Composite Struct.*, vol. 93, no. 5, pp. 1328–1336, 2011.
- [3] P. Gaudenzi, M. Bernabei, E. Dati, G. de Angelis, M. Marrone, and L. Lampani, "On the evaluation of impact damage on composite materials by comparing different NDI techniques," *Composite Struct.*, vol. 118, no. 1, pp. 257–266, 2014.
- [4] J. Jebramcik, I. Rolfes, N. Pohl, and J. Barowski, "Millimeterwave radar systems for in-line thickness monitoring in pipe extrusion production lines," *IEEE Sens. Lett.*, vol. 4, no. 5, pp. 1–4, May 2020.
- [5] D. Meier *et al.*, "Millimeter-wave tomographic imaging of composite materials based on phase evaluation," *IEEE Trans. Microw. Theory Techn.*, vol. 67, no. 10, pp. 4055–4068, Oct. 2019.
- [6] N. S. Schreiner, W. Sauer-Greff, R. Urbansky, G. von Freymann, and F. Friederich, "Multilayer thickness measurements below the rayleigh limit using FMCW millimeter and terahertz waves," *Sensors*, vol. 19, no. 18, pp. 3910:1–3910:13, Sep. 2019.
- [7] G. Chen, L. Fu, K. Chen, C. D. Boateng, and S. Ge, "Adaptive ground clutter reduction in ground-penetrating radar data based on principal component analysis," *IEEE Trans. Geosci. Remote Sens.*, vol. 57, no. 6, pp. 3271–3282, Jun. 2019.
- [8] F. H. C. Tivive, A. Bouzerdoum, and M. G. Amin, "A subspace projection approach for wall clutter mitigation in through-the-wall radar imaging," *IEEE Trans. Geosci. Remote Sens.*, vol. 53, no. 4, pp. 2108–2122, Apr. 2015.
- [9] D. Meier *et al.*, "Propagation of millimeter waves in composite materials," *IEEE Trans. Antennas Propag.*, vol. 68, no. 4, pp. 3080–3093, Apr. 2020.
- [10] S. Scherr *et al.*, "Influence of radar targets on the accuracy of FMCW radar distance measurements," *IEEE Trans. Microw. Theory Techn.*, vol. 65, no. 10, pp. 3640–3647, Oct. 2017.
- [11] T. Merkle *et al.*, "Broadband 240-GHz radar for non-destructive testing of composite materials," *IEEE J. Solid-State Circuits*, vol. 54, no. 9, pp. 2388–2401, Sep. 2019.
- [12] R. Weber *et al.*, "A W-band x12 frequency multiplier MMIC in waveguide package using quartz and ceramic transitions," in *Proc. IEEE Compound Semicond. Integr. Circuit Symp.*, 2011, pp. 1–4.
- [13] A. Leuther *et al.*, "Metamorphic HEMT technology for low-noise applications," in *Proc. IEEE Int. Conf. Indium Phosphide Related Mater.*, 2009, pp. 188–191.